Eco-Friendly Hydrogel from Sodium Alginate and Orange Peel for Sustainable Soil Conditioning

Hajaratul Najwa Mohamed[1*], Che Ku Mohd Faizuldin Che Ku Mohd Yassin[1], Nabihah Abdullah[1], Norazlina Hashim[1], Shuhaimi Mustafa[2], and Abdul Fattah Ab Razak[3]

[1]*Department of Natural Resources and Environment, Faculty of Engineering Technology, University College TATI, Jl. Panchur, Teluk Kalong, 24000 Kemaman, Terengganu, Malaysia*

[2]*Halal Product Research Institute, Putra Infoport, Universiti Putra Malaysia, 43400 UPM Serdang, Selangor, Malaysia*

[3]*Department of Food Technology, School of Engineering and Technology, University of Technology Sarawak, Jl. Universiti No. 1, 96000 Sibu, Sarawak, Malaysia*

* ***Corresponding author:***

tel: +609-8601000
email: hnajwa@uctati.edu.my

Received: September 14, 2025
Accepted: November 12, 2025

DOI: 10.22146/ijc.111205

Abstract: *An eco-friendly hydrogel was developed from sodium alginate (ALG) and orange peel (OP) powder through ionotropic gelation for application as a sustainable soil conditioner. Limonene (LMN) at 1.5 wt.% was incorporated to enhance the functional properties of the hydrogel. Fourier-transform infrared spectroscopy (FTIR) results confirmed the successful integration of OP into the ALG network through the presence of characteristic hydroxyl and carboxyl functional groups, while thermogravimetric analysis indicated improved thermal stability with increasing OP content due to its lignocellulosic reinforcement. Swelling analysis revealed that the incorporation of 5 wt.% OP enhanced the swelling capacity to 95.5% compared to 65.8% for ALG–LMN alone. However, further increases in OP content (10–15 wt.%) reduced swelling, suggesting excessive filler restricted water diffusion and polymer relaxation. Lower OP concentrations (1–3 wt.%) maintained high water absorption and structural integrity. These findings demonstrate that moderate OP incorporation optimizes the balance between water retention and mechanical stability, indicating strong potential of the ALG–OP–LMN hydrogel as a biodegradable and sustainable soil conditioning material that valorizes agricultural waste.*

Keywords: *hydrogel; sodium alginate; orange peel; soil conditioning*

■ INTRODUCTION

According to Saleem et al. [1], current agricultural model practices lack sustainability and pose a threat to the planet's future due to water constraints, biodiversity loss, soil quality degradation, and excessive greenhouse gas emissions. It is a vast and complex task that can be approached in various ways to make the present agricultural systems more efficient and sustainable. Soil conditioners are among the new materials that show enormous promise for that use. Soil conditioners are products that, in general, help retain water, preserve soil nutrients, and maintain soil structure while improving crop yields [2]. Hydrogels appear to be the most promising material for tackling this challenge due to their ability to retain water for a prolonged period through their swelling properties. The unique characteristic of a hydrogel is that it can hold a significant amount of water within its three-dimensional network and release it when the plant and its environment need it. Using hydrogels enhances soil porosity and water retention capacity, providing plants with humidity and a favorable environment for root growth. All these factors eventually boost agricultural yields. Additionally, hydrogel helps manage irrigation water more effectively [3].

Hydrogels derived from natural polymers have gained prominence in recent studies due to their

applications in the food industry [4], agriculture, and pharmaceuticals [5-7]. Among the available options, polysaccharides are often favored over synthetic alternatives due to their merit characteristics. Extensive research has focused on the development of innovative hydrogel structures by integrating both synthetic polymers and polysaccharides. Among the commonly investigated polysaccharides are chitosan [8-9], alginate [7,10-12], starch [13-15], cellulose [16], carboxymethylcellulose [17-18], and hyaluronic acid [19]. The natural polysaccharides offer a range of appealing properties, including renewability, cost-effectiveness, abundance, biodegradability, multifunctionality, strong reactivity, and versatile adsorption capabilities [13,20-21]. Consequently, interest in fabricating hydrogels from biopolymeric sources has seen a notable increase in recent years.

Sodium alginate (ALG) was selected as the base polymer for synthesizing functional hydrogels due to its exceptional gel-forming abilities and potential for mass production. This naturally occurring polysaccharide originates from brown marine algae and exists in the form of a water-soluble alginic acid salt. Composed of β-D-mannuronic and α-L-guluronic units joined by 1,4-glycosidic bonds, its molecular structure accounts for its recognized non-toxic behavior. As noted by dos Santos [22], ALG polymers allow for the rearrangement of mannuronic and guluronic acid sequences along their chains. The most crucial characteristic of ALG is its capacity to gel when cross-linking agents, or divalent cations, such as Ca^{2+} ions, are present. Hydrogel networks can be formed through the ionotropic gelation mechanism, in which anionic ALG chains interact with multivalent inorganic cations [23].

The petroleum-derived and non-biodegradable polymers used in commercial hydrogels for this purpose include polyacrylate and polyacrylamide. Therefore, considerable scientific effort has been devoted in recent decades to finding biodegradable substitutes for these commercial hydrogels. However, problems such as the hydrogels' inadequate degradability and the resulting production of micro- or nanoplastics remain unresolved. The use of acrylates and acrylamide monomers as cross-linkers in polymer systems is a common practice [24-26]. Thus, by employing natural biodegradable substances and upcycling industrial vegetable waste, this effort aims to provide an efficient and eco-friendly alternative to commercial hydrogels.

Citrus sinensis, commonly known as the orange, represents approximately 60% of global citrus production and is the most widely consumed citrus fruit. In 2020 alone, worldwide orange production exceeded 75 million metric tons. Of this total, about 18% was allocated for industrial juice manufacturing, resulting in orange peel (OP) as the major agro-waste, comprising roughly 45% of the total processed mass [27]. OP contains a diverse array of bioactive compounds, including flavonoids, essential oils, polyphenols, and a variety of micro- and macronutrients. Additionally, it contains pectin, a structurally complex hetero-polysaccharide primarily composed of α-D-galacturonate residues linked at the 1,4-position, with partial methyl esterification. Notably, R-(+)-limonene (LMN) is the predominant component in orange essential oil. Due to its beneficial roles in agriculture—such as insect repellency and biopesticidal activity—LMN was incorporated into the hydrogel formulation to potentially enhance plant defense mechanisms [28]. To avoid phytotoxicity, the applied concentration was carefully limited to 1.5 wt.% [29]. It is also important to highlight that LMN is recognized for its non-toxic, as well as promising anti-inflammatory, antioxidant, and antitumor activities [30].

This study aims to design and evaluate alginate–orange peel hydrogels containing limonene (ALG-OP-LMN) as potential soil conditioners, employing physicochemical and morphological analyses. Specifically, Fourier-transform infrared spectroscopy (FTIR), thermogravimetric analysis (TGA), scanning electron microscopy (SEM), and swelling studies were conducted to evaluate the structural, thermal, morphological, and swelling properties, respectively, of the formulated hydrogels. The possible advantages of this research are substantial. The agricultural sector can significantly reduce its environmental impact, address water scarcity, prevent soil degradation, and contribute

to the overarching goal of establishing a more sustainable and resilient food system by developing sustainable and biodegradable soil conditioners. Furthermore, utilizing industrial vegetable waste as a primary ingredient for these soil conditioners can contribute to waste reduction and foster a more sustainable circular economy.

■ EXPERIMENTAL SECTION

Materials

Tween 80, LMN, and analytical grade ALG powder were acquired from Sigma-Aldrich. Calcium chloride ($CaCl_2$) was purchased from Merck (Germany).

Instrumentation

The FTIR analysis was performed with a VERTEX 70v spectrometer (Bruker, Germany). The thermal behavior and decomposition profile of the synthesized hydrogels were investigated using TGA (Hitachi STA7200). The morphology properties of the hydrogel were analyzed using SEM (JEOL JSM-IT200).

Procedure

Experimental design

The experimental design was structured in two main stages: screening experiments and subsequent characterization studies. The screening experiments were conducted to identify suitable composition ranges of ALG and OP polymers capable of forming stable and homogeneous hydrogels. Only formulations that produced well-formed hydrogels were selected for further characterization and analysis. The screening outcomes were used to determine the suitable compositional range of ALG and OP for the next experimental phase, focusing on detailed characterization of structural, thermal, morphology, and swelling properties.

Synthesis and pretreatment of OP powder

C. sinensis (sweet orange) peels were initially cleaned using tap water to eliminate surface residues. The cleaned peels were then exposed to sunlight for 20 h to undergo preliminary drying, followed by further dehydration for 18 h in an oven at 60 °C, as outlined by Farahmandfar [31]. Once dried, OP was manually broken down using a pestle and mortar, then finely ground using a blender. The obtained material was subjected to mechanical sieving to achieve a uniform particle size of 100 μm. OP powder (1.5 g) was combined with 100 mL of distilled water to prepare an OP stock solution at a concentration of 1.5 wt.%. The solution was maintained under stirring at 500 rpm (90 °C) for 15 min to form a suspension.

LMN nanoemulsion preparation

By implementing certain modifications, LMN nanoemulsion was carried out as described by Silva et al. [32]. For the preparation of a 1.5 wt.% LMN nanoemulsion, LMN (0.75 g) was dispersed in 50 mL of distilled water, with Tween 80 employed as an emulsifying agent at a concentration of 0.5 wt.% relative to the LMN.

Preparation of ALG-OP hydrogel

ALG-OP hydrogels incorporating LMN were synthesized using a modified ionic gelation technique [33], which relies on the binding of ALG with Ca^{2+} supplied by a $CaCl_2$ solution. ALG powder, OP powder, and LMN oil were used as the primary materials, with Tween 80 (0.5 wt.%) serving as a surfactant to stabilize the oil phase. The formulation matrix consisted of ALG (1–2 wt.%), OP (5–15 wt.%), and a constant LMN concentration of 1.5 wt.%, with the total batch mass fixed at 50 g for each sample (Table 1). In a typical preparation, the required amounts of ALG and OP powders were weighed and premixed in a 100 mL beaker to ensure uniform dispersion. Approximately 80% of the total distilled water was then added, and the mixture was stirred at 600 rpm for 30 min to allow partial hydration of ALG. Subsequently, LMN (1.5 wt.%) and Tween 80 (0.25 g per 50 g batch) were added dropwise under continuous stirring to form a stable emulsion. The remaining water was then added to achieve a total mass of 50 g, and the mixture was stirred for an additional 30 min until a homogeneous, viscous solution was obtained.

For hydrogel bead formation, the prepared emulsions were extruded dropwise into a 0.2 M $CaCl_2$ cross-linking bath using a 5 mL syringe. The beads were allowed to harden for 24 h before being washed with

Table 1. Samples' compositions in the screening experiment

Sample ID	ALG (wt.%)	OP (wt.%)	LMN (wt.%)	ALG (g)	OP (g)	LMN (g)	Distilled water (g)
S1	1.0	0	1.5	0.50	0	0.75	46.00
S2	1.0	5	1.5	0.50	2.50	0.75	43.50
S3	1.0	10	1.5	0.50	5.00	0.75	41.00
S4	1.0	15	1.5	0.50	7.50	0.75	45.75
S5	1.5	0	1.5	0.75	0.00	0.75	43.25
S6	1.5	5	1.5	0.75	2.50	0.75	40.75
S7	1.5	10	1.5	0.75	5.00	0.75	45.25
S8	1.5	15	1.5	0.75	7.50	0.75	42.75
S9	2.0	0	1.5	1.00	0	0.75	40.25
S10	2.0	5	1.5	1.00	2.50	0.75	44.75
S11	2.0	10	1.5	1.00	5.00	0.75	42.25
S12	2.0	15	1.5	1.00	7.50	0.75	39.75

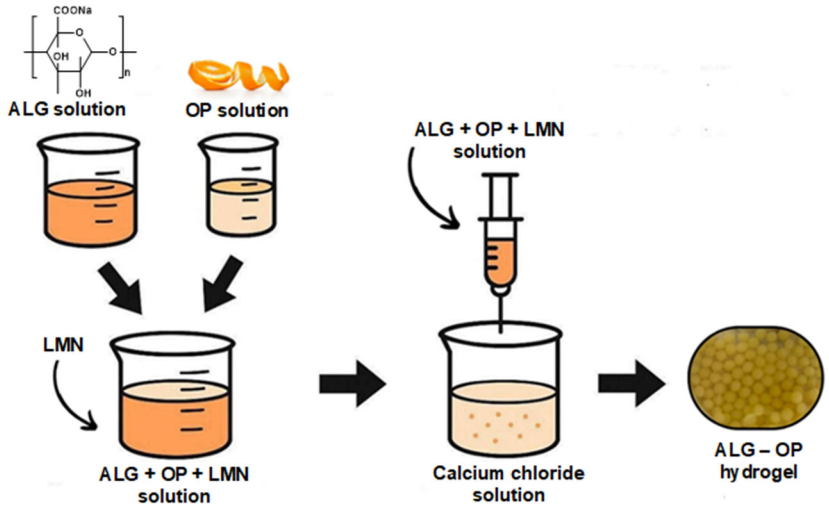

Fig 1. Schematic representation of ALG–OP hydrogels preparation through the ionic gelation method

distilled water to remove excess Ca^{2+}, and stored in a chiller for further characterization. The overall procedure is illustrated schematically in Fig. 1, showing the sequence of dispersion, emulsion formation, and ionotropic gelation steps leading to the formation of ALG–OP–LMN hydrogel beads. Each formulation was assessed for bead formation quality based on visual appearance, shape retention, and structural integrity.

Table 1 lists the weight percentages and corresponding masses of ALG, OP, and LMN for each sample, assuming a total mass of approximately 50 mL or 50 g. The diameter of the hydrogel beads was measured using a digital caliper with a precision of ± 0.01 mm. A total of fifty beads were randomly selected and measured in their hydrated state immediately after gelation to determine the average bead size. The mean diameter and standard deviation were calculated and reported as the size dimension of the hydrogels.

Characterizations of hydrogels using FTIR

The FTIR spectral data were collected between 4000 and 600 cm^{-1}, using a resolution of 4 cm^{-1} and an accumulation of 64 scans. The thermal behavior and decomposition profile of the synthesized hydrogels were investigated using TGA. In this method, approximately 18.5 mg of sample was placed into a sample pan and subjected to a controlled heating program, where the temperature was gradually increased from 30 to 600 °C at a constant heating rate of 10 °C/min, under a continuous flow of high-purity nitrogen gas at a rate of 50 mL/min.

Morphological properties of hydrogel using SEM

Hydrogel samples were soaked in tap water for 24 h to achieve swelling before microstructural examination. They were then subjected to freeze-drying for an additional 24 h using a CHRIST Epsilon 2–4 LSCplus lyophilizer (Germany), operated at 10 °C and 1.14 mbar. After drying, the hydrogels were cryo-fractured by immersing them in liquid nitrogen. The fractured surfaces were subsequently mounted onto aluminum stubs using conductive carbon tape. A thin gold layer (~10 nm) was applied via sputter coating to enhance conductivity. Microstructural characterization was performed using SEM operated at 10 kV and 78 μA with a secondary electron imaging (SEI) detector. SEM images were acquired at magnifications of 500×, 2500×, and 5000×

Swelling properties of hydrogel

The swelling properties of the hydrogels were assessed by determining the mass variation before and after immersion in distilled water. To begin, the samples were oven-dried under vacuum at 40 °C overnight, and their initial mass, W_i was recorded using an analytical balance. The dried samples were subsequently soaked in distilled water at ambient temperature (20 °C) for 24 h. Following swelling, excess surface water was carefully removed with tissue paper, after which the final mass, W_f was measured. The degree of swelling was then calculated according to Eq. (1). All samples were analyzed in duplicate, and the results are presented as average ± SD.

$$\text{Swelling}\% = \frac{W_f - W_i}{W_i} \times 100\% \quad (1)$$

Statistical analysis

To evaluate differences among normally distributed data sets, a one-way ANOVA was applied. Tukey's post-hoc test was performed for pairwise comparisons between group means. Statistical significance was considered at $p < 0.05$. All analyses were executed using MINITAB software, version 16 (Minitab Inc., Pennsylvania, USA).

■ RESULTS AND DISCUSSION

ALG-OP Hydrogel Formation

A preliminary screening experiment was conducted to determine the suitable composition range of ALG and OP for forming well-structured hydrogel beads via ionotropic gelation. The results are summarized in Table 2. Hydrogel beads were assessed based on their ability to form spherical shapes and maintain mechanical integrity after crosslinking in 0.2 M $CaCl_2$ solution. Bead formation was successfully achieved for formulations containing 1–2 wt.% ALG with up to 10 wt.% OP. The well-formed ALG–OP hydrogel beads exhibited a nearly spherical shape with an average diameter of 2.1 ± 0.3 mm, as determined using a digital caliper (± 0.01 mm accuracy). At higher OP loadings (15 wt.%), the beads lost shape and became irregular, indicating that excessive OP disrupted the ionic cross-linking process. The images of produced hydrogels are shown in Fig. 2.

Table 2. 1st trial of hydrogel formation using ALG and OP

Sample	ALG (wt.%)	OP (wt.%)	Result
S1	1.0	0	Beads well formed
S2	1.0	5	Beads well formed
S3	1.0	10	Beads well formed
S4	1.0	15	Beads are not well formed
S5	1.5	0	Beads well formed
S6	1.5	5	Beads well formed
S7	1.5	10	Beads well formed
S8	1.5	15	Beads are not well formed
S9	2.0	0	Beads well formed
S10	2.0	5	Beads well formed
S11	2.0	10	Beads are not well formed
S12	2.0	15	Beads are not well formed

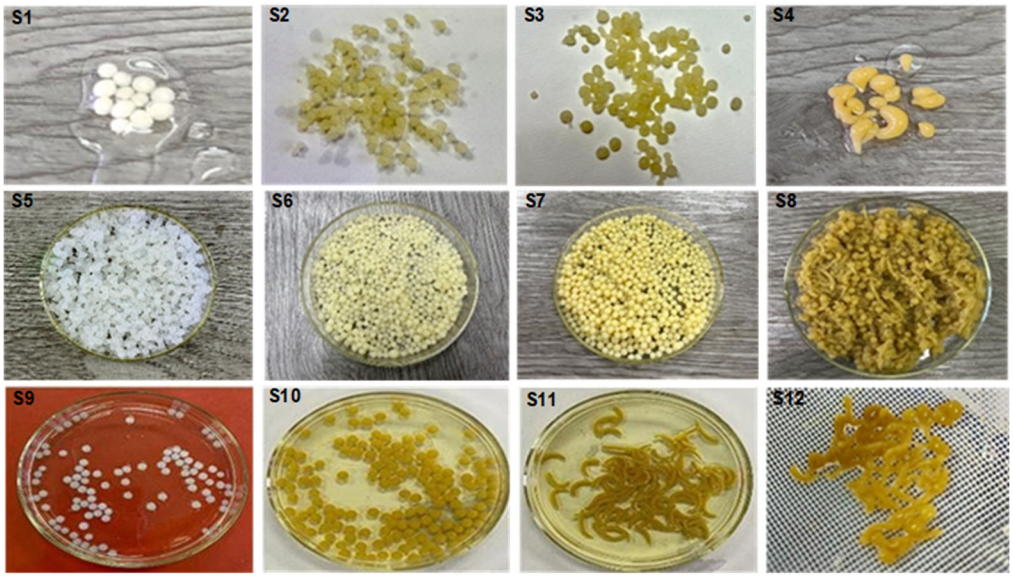

Fig 2. The images of hydrogel formation in the screening experiment

Although 1 wt.% ALG produced visually well-formed beads, these hydrogels were mechanically weak and fragile, easily deforming under gentle handling. This fragility likely resulted from an insufficient density of cross-linked ALG chains, leading to a weak gel network. In contrast, increasing the ALG concentration to 1.5–2.0 wt.% improved the bead integrity and cohesion, resulting in stronger hydrogel structures with higher gel rigidity. Similar effects of ALG concentration on gel strength have been reported in previous studies [34-35]. The viscosity of ALG enables it to influence the shape of the beads produced, with a higher concentration of ALG producing more spherical beads. However, essentially, an ALG solution with a concentration greater than 5 wt.% is challenging to formulate due to the increased viscosity [33]. At higher OP content (≥ 10 wt.%), bead formation was poor and nonuniform. The high solid load of OP powder increased the viscosity and heterogeneity of the mixture, limiting the diffusion of Ca^{2+} ions into the ALG matrix. Furthermore, components of OP, such as cellulose, hemicellulose, and pectin, may compete for water and physically interfere with ALG chain interactions, leading to irregular gelation [35].

Additionally, OP contains bioactive compounds such as polyphenols and flavonoids, which may interact with ALG molecules and disrupt the typical gelation process. These interactions could weaken or alter the cross-linking network, reducing the ability of the hydrogel droplets to maintain a spherical shape upon gelation. The presence of these compounds could also influence the interfacial tension between the hydrogel precursor solution and the gelling medium, contributing to irregular or deformed hydrogel structures [36]. Another factor to consider is the impact of OP particles on the stability of hydrogels and droplet formation prior to gelation. At high OP concentrations, solid particles may interfere with the formation of uniform droplets, resulting in irregularities in shape during the gelation process. In some cases, particle aggregation could also create localized variations in gel strength, resulting in non-spherical hydrogels. Overall, the findings suggest that while the addition of OP can improve the functional properties of ALG hydrogels, excessive OP content negatively impacts hydrogel morphology. Therefore, based on these results, formulations with ALG at 1.5 wt.% and OP at 5–10 wt.% were identified as optimal for subsequent experiments.

Physicochemical Characterization of Hydrogels

To gain a deeper insight into the interactions that occur between OP, LMN, and ALG, characterization was conducted using three principal techniques: FTIR, TGA, and SEM.

FTIR

The FTIR spectra yielded insights into the functional groups and molecular-level properties of the hydrogel constituents. The FTIR spectra of 1.5 wt.% ALG + (5–15 wt.%) OP + LMN are shown in Fig. 3, and all samples display prominent peaks at 3400 cm^{-1}, representing the stretching vibrations of hydroxyl (OH) groups. Belattmania et al. [37] analyzed ALG extracted from brown seaweeds and reported similar absorption bands at 3200–3400 cm^{-1}, which were attributed to O–H stretching vibrations. Meanwhile, at 1700 cm^{-1}, which can be ascribed to the carbonyl (C=O) stretching of the carboxylate groups in the ALG backbone. The observed characteristics align with the established chemical structure of ALG, verifying its existence as a primary constituent in this hydrogel composition [38]. Distinct peaks were observed at 1600 and 1400 cm^{-1} across all samples, corresponding to the asymmetric and symmetric stretching vibrations of carboxylate (COO^-) groups, which are characteristic of ALG. These functional groups play a vital role in ionic cross-linking and gel network formation, with their intensities reflecting the extent of gel stretching [39]. In addition, a strong C–O stretching band near 1040 cm^{-1} confirmed the presence of polysaccharides [37,39].

The FTIR spectrum of the ALG + 5 wt.% OP + LMN hydrogel revealed additional peaks at 2920 and 2850 cm^{-1}, corresponding to the stretching vibrations of aliphatic C–H groups. The presence of these signals indicates the successful integration of OP component, which contains LMN and other terpene chemicals, into the hydrogel matrix. In addition, the FTIR analysis of the incorporation of 10–15 wt.% OP into the ALG hydrogel indicated a stronger intensity of the aliphatic C–H peaks, suggesting a higher concentration of chemicals derived from OP in this formulation.

In the hydrogels containing OP, the C=O stretching band remains visible, while a new peak appears at 1708 cm^{-1}, corresponding to the C=O stretching vibration of free COOH groups. This peak is specifically attributed to the demethoxylation of pectin [40]. Additionally, the O–H stretching band of ALG at 3358 cm^{-1} exhibited a significant increase in intensity upon incorporation of OP in different concentrations. This suggests the formation of new hydrogen bonds, particularly in hydrogels composed of both ALG and OP. Furthermore, the bands at 1013, 1145, and 1050 cm^{-1} in ALG-OP are characteristic of pectin homogalacturonan structures, indicating the release of pectin polymers from the plant cell wall [41]. The presence of ALG-specific functional groups, combined with the incorporation of chemicals derived from OP, reinforces the previously observed swelling and solubility properties. The heightened strength of the aliphatic C–H signals, in correlation with increased OP content, provides further evidence that OP component influences the hydrogel's ability to retain water.

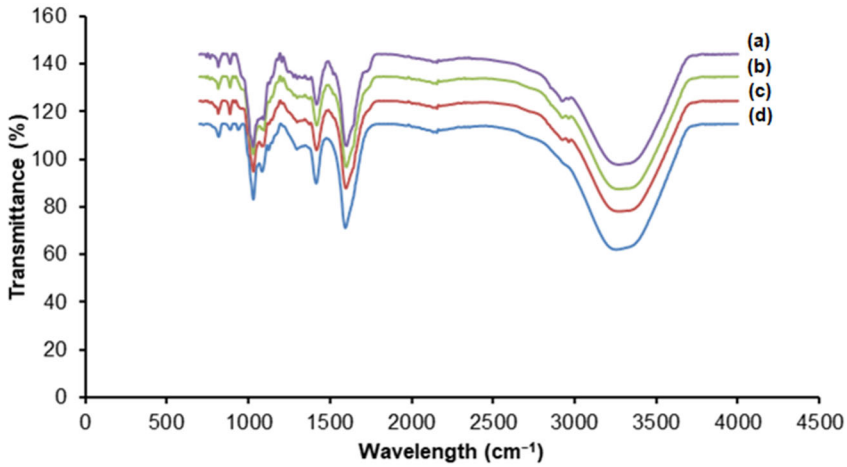

Fig 3. FTIR spectra of (a) ALG + 15 wt.% OP + LMN, (b) ALG + 10 wt.% OP + LMN, (c) ALG + 5 wt.% OP + LMN, and (d) ALG + LMN, confirm the presence of significant peaks and interactions among functional groups

TGA

TGA was performed to evaluate the response of the hydrogel to heat and to determine the interactions between its components. Based on Fig. 4(a), in the initial heating stage, between approximately 30 and 120 °C, all samples exhibited a steep decline in weight. This was primarily attributed to the evaporation of physically adsorbed moisture and the loss of loosely bound water molecules within the hydrogel structure. The rate and extent of this early weight loss were similar for all samples, suggesting comparable moisture content at the start. Between 120 and 250 °C, a more pronounced degradation stage occurred. This phase was typically associated with the decomposition of low-molecular-weight organic components, such as residual polysaccharides, and the breakdown of weaker chemical bonds within the hydrogel matrix [42]. In this region, ALG + 10 wt.% OP + LMN and ALG + 15 wt.% OP + LMN samples demonstrated a slower degradation rate compared to ALG + LMN and ALG + 5 wt.% OP + LMN, which experienced a faster weight drop to below 20%. This indicates that ALG hydrogels with a higher content of OP have greater resistance to decomposition at moderate temperatures. Beyond 250 °C and up to around 600 °C, the curves show a gradual weight loss corresponding to the breakdown of the main polymer backbone, including ALG, cellulose, and lignin components from OP filler [36]. In this final stage, the differences between samples become clearer in terms of residual mass. Hydrogel with 15 wt.% OP retains the highest residual weight, at approximately 17–18%, followed by ALG + 10 wt.% OP at around 12–13%. In contrast, the other samples leave behind significantly less residue, ranging from 6 to 8%. A higher residual mass at elevated temperatures is generally indicative of greater thermal stability and a higher proportion of thermally stable inorganic components.

Differential thermogravimetry (DTG) result, as shown in Fig. 4(b), revealed that Samples 1 (ALG + LMN) and 2 (ALG + 5 wt.% OP + LMN) exhibit their principal mass-loss rate at approximately 90 °C, consistent with desorption of water and loss of light volatiles. Sample 3 (ALG + 10 wt.% OP + LMN) displays a strong DTG peak at approximately 177 °C, indicating a distinct higher-temperature decomposition event likely related to orange-peel constituents or interactions between OP and ALG matrix [43]. Sample 4 (ALG + 15 wt.% OP + LMN) exhibits a dominant DTG peak at approximately 80 °C, indicating that a low-temperature volatile/moisture loss is the dominant process in that sample. These results indicate that the inclusion and amount of OP can significantly alter thermal behavior; however, the trend is not strictly monotonic with OP loading and may reflect differences in moisture, sample heterogeneity, or overlapping degradation processes.

SEM

SEM examination was conducted to examine the surface morphology and microstructural characteristics of the hydrogel samples. The morphology images of the ALG + LMN hydrogel are shown in Fig. 5(a), where the exterior exhibits a creased and porous texture, characterized by interconnected networks within the

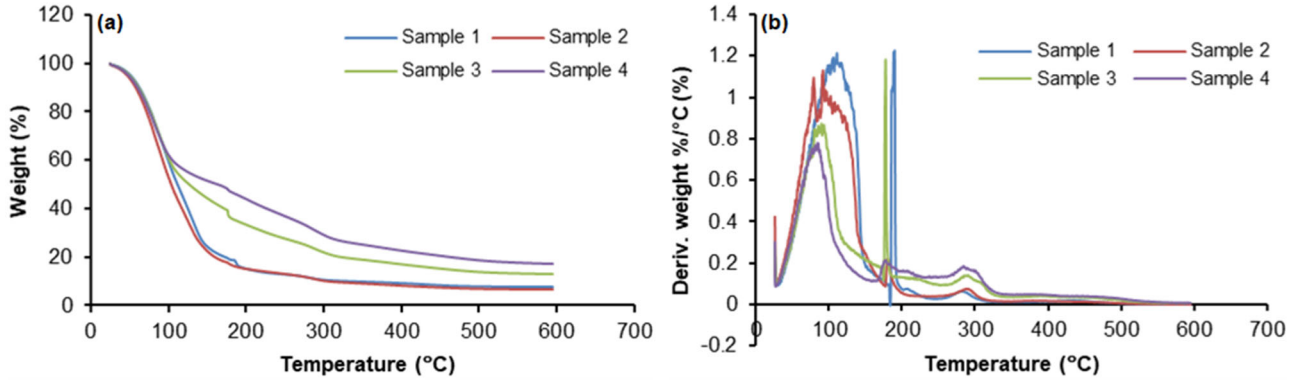

Fig 4. (a) TGA and (b) DTG of Sample 1: ALG + LMN, Sample 2: ALG + 5wt.% OP, Sample 3: ALG + 10 wt.% OP, Sample 4: ALG + 15 wt.% OP

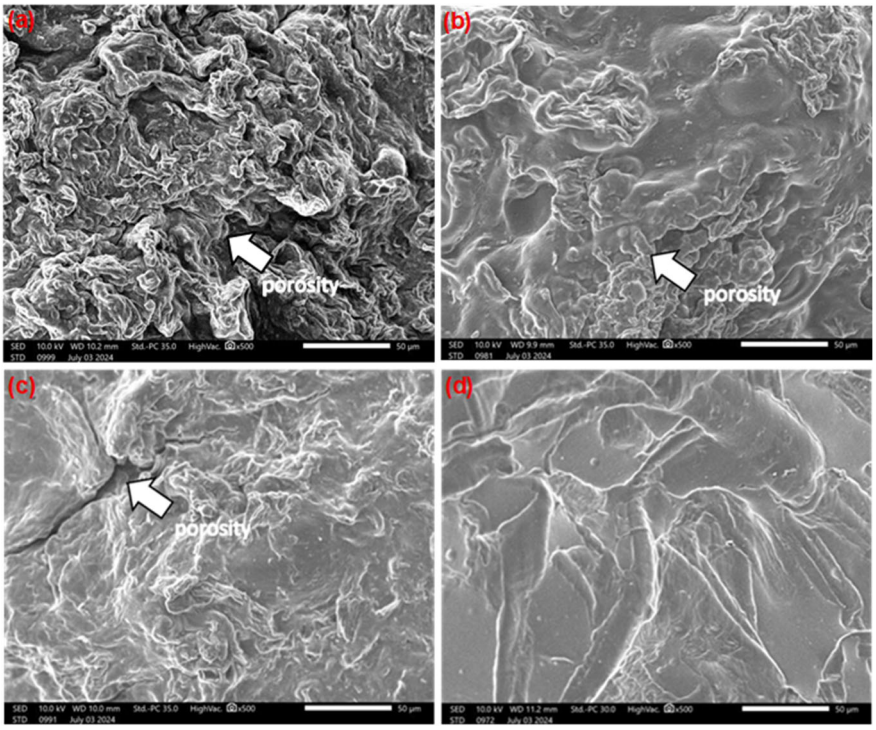

Fig 5. SEM micrographs of (a) ALG + LMN, (b) ALG + 5wt.% OP + LMN, (c) ALG +10 wt.% OP + LMN, (d) ALG + 15 wt.% OP + LMN. SEM micrographs were acquired at 500× magnification, and the scale bar is 50 μm

pores, while the surface topology reveals a rough texture. The proliferation of channels and gaps likely resulted in an augmented surface area and enhanced pathways for water infiltration and retention within the hydrogel structure. The shape of this hydrogel composition aligns with ALG's notable characteristics, including a high swelling capacity and water retention qualities [44].

On the other hand, the SEM images of the ALG + 5 wt.% OP + LMN hydrogel in Fig. 5(b) exhibited a surface structure that was both porous and heterogeneous. The inclusion of the OP component seems to create abnormalities and interconnecting channels within the hydrogel matrix. The presence of this porous microstructure is likely responsible for the water absorption and swelling capacity of this formulation. A porous structure provides a large internal surface area, increasing the number of contact points for water molecules to interact with the material's hydrophilic polymer chains [45]. Increasing the OP content to 10% as shown in Fig. 5(c), resulted in the formation of a reduced porosity system with smaller and fewer channels throughout the hydrogel.

In contrast, after adding 15 wt.% OP, the hydrogel exhibited a reasonably smooth and uniform surface topography, with minimal observable pores or channels, as shown in Fig. 5(d). Interestingly, filamentous formations were observed at both the macroscopic and microscopic levels. This phenomenon was likely due to the release of pectin and hemicelluloses through a chemical cross-linking process, resulting in the formation of filamentary structures that were observed as a second phase. OP is rich in pectin, which also cross-links with Ca^{2+} (similar to ALG) via the "egg-box" model. At higher concentrations, mixed ALG–pectin junction zones can form denser, oriented polymer domains that may appear filamentous [46]. These findings are consistent with those of Merino et al. [36], who reported a reduction in swelling capacity after incorporating a higher OP content into an agar matrix. Integrating the SEM analysis into the results and discussion section enhances the overall comprehension of the hydrogel's microstructural characteristics and their correlation with the observed physical and functional attributes. The visual characterization, in

conjunction with the preceding FTIR analysis, provides a comprehensive view of the hydrogel's composition, structure, and performance attributes.

Swelling Study of Hydrogels

The swelling ability of hydrogels is a crucial parameter, as it reflects both the hydrophilic characteristics of the polymer matrix and the extent of cross-linking within the network. Generally, a more densely cross-linked structure restricts water uptake, resulting in reduced swelling. Swelling behavior can therefore be used to evaluate batch uniformity and production quality, while also providing insight into potential changes in the material's mechanical performance over time. Hydrogels composed of lightly cross-linked, water-affinitive polymers typically exhibit rapid swelling upon contact with water. This property is attributed to the presence of hydrogen-bonded polymer chains that form a three-dimensional network (macroreticular structure) capable of retaining large quantities of water [47]. Fig. 6 shows the hydrogels during the swelling studies.

The swelling behavior of the ALG–OP hydrogels incorporated with LMN exhibited a strong dependence on the concentration of OP powder within the polymer matrix. The control hydrogel containing only ALG and LMN showed a swelling ratio of 65.8%. The incorporation of 5 wt.% OP significantly enhanced the swelling to 95.5%, indicating that a small amount of OP promoted water uptake within the hydrogel network. This enhancement can be attributed to the hydrophilic nature of polysaccharides, such as pectin and cellulose, present in OP, which introduces additional OH and COOH groups capable of forming hydrogen bonds with water molecules [48]. Moreover, partial chelation of Ca^{2+} by acidic components in OP could have reduced the effective cross-linking density, allowing the hydrogel matrix to expand more freely [49].

However, further increases in OP loading to 10 and 15 wt.% led to a substantial reduction in swelling (57.5 and 42.9%, respectively). The decline in swelling capacity at higher OP content is likely due to the excessive incorporation of insoluble fibrous materials, which restricts chain mobility and reduces the free volume available for water diffusion. The dense packing of cellulose and lignin components may also contribute to a more rigid structure, limiting the hydrogel's ability to expand. Additionally, higher filler loading could hinder uniform dispersion of OP within the ALG network, resulting in heterogeneous cross-linking and reduced water accessibility. Aarstad et al. [50] reported the work on ALG–cellulose nanofibril (CNF) composites where the addition of CNF to Ca-ALG gels led to a concentration-dependent decrease in syneresis (volume shrinkage) and reduced swelling (increased dimensional stability) as filler content increased.

To better understand the role of OP concentration, lower OP contents (1 and 3 wt.%) were subsequently investigated. The swelling capacity for these hydrogels increased to 84.8 and 90.7%, respectively, confirming that moderate OP incorporation enhances water absorption without severely compromising the structural integrity of the hydrogel. These results suggest that an optimum range of OP concentration (approximately 3–5 wt.%) promotes hydrophilicity and

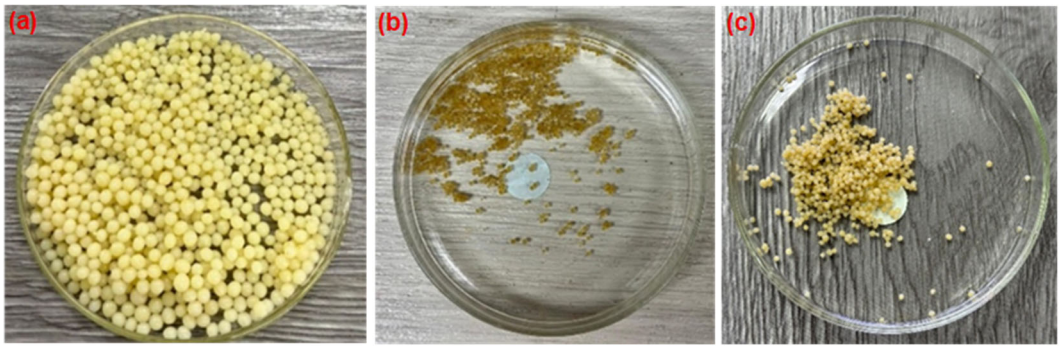

Fig 6. The ALG-OP hydrogels during swelling test: (a) hydrogel in hydrated state after gelation, (b) hydrogel after drying process for 24 h, and (c) the swollen hydrogel after 24 h of swelling process

network porosity, while excessive OP loading introduces a filler-dominated effect that suppresses swelling. Fig. 7 shows the effect of OP concentration on the swelling percentage of 1.5 wt.% ALG hydrogels. The swelling increased with the incorporation of low OP content (1–5 wt.%), reaching a maximum of 95.5% at 5 wt.% OP, and subsequently decreased at higher OP loadings (10–15 wt.%). The trend indicates an optimum OP concentration for enhancing water absorption, beyond which excessive fibrous filler restricts the expansion of the hydrogel network.

Furthermore, the review of cellulose-based hydrogels indicates that fillers/fibers often reduce swelling when used beyond optimal loadings because they reduce effective pore size or occupy water-absorbing network sites [51]. In this system, the presence of LMN may further complicate interactions by altering the hydrophobic or hydrophilic balance and affecting the network microstructure, but the dominant effect appears to be OP loading. The reduction aligns with the FTIR results, which indicate the presence of pectin in the hydrogel network. The ionic cross-linking between ALG and OP mostly released pectin polymer, resulting in the production of filamentous structures devoid of porosity, as observed in SEM analysis. In summary, the results are consistent with prior literature on ALG–filler systems: hydrophilic natural fillers at low levels can enhance water uptake, but at higher levels they restrict network expansion and water diffusion.

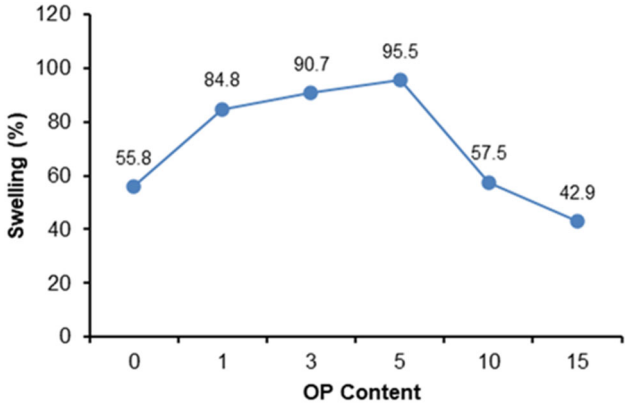

Fig 7. Swelling percentage of ALG–OP hydrogels incorporated with LMN

■ CONCLUSION

The incorporation of OP into ALG hydrogels significantly impacted their swelling, thermal, and structural properties. The results established that moderate OP concentrations (3–5 wt.%) significantly improved water absorption and network porosity, whereas higher OP loadings led to reduced swelling due to limited polymer mobility and densified structure. FTIR and SEM analyses confirmed the successful integration of OP and the formation of a porous microstructure, while TGA revealed enhanced thermal resistance with increasing OP content. Overall, the optimized ALG–OP–LMN hydrogel presents a promising biodegradable alternative to synthetic soil conditioners, enhancing soil moisture retention and promoting sustainable waste utilization in agricultural applications.

■ ACKNOWLEDGMENTS

This research was funded by University College TATI (Short Term Grant, GPJP 9001:2402).

■ CONFLICT OF INTEREST

The authors have no conflict of interest.

■ AUTHOR CONTRIBUTIONS

Hajaratul Najwa Mohamed led the analysis and writing of the paper. Che Ku Mohd Faizuldin Che Ku Mohd Yassin conducted the experiments. Nabihah Abdullah performed the swelling calculations. Norazlina Hashim contributed to the interpretation of the results. Shuhaimi Mustafa participated in analysis discussions and refinement of the study conclusions, and Abdul Fattah Ab Razak reviewed and revised the manuscript. All authors approved the final version of this manuscript.

■ REFERENCES

[1] Saleem, A., Anwar, S., Nawaz, T., Fahad, S., Saud, S., Ur Rahman, T., Khan, M.N.R., and Nawaz, T., 2025, Securing a sustainable future: The climate change threat to agriculture, food security, and sustainable development goals, *J. Umm Al-Qura Univ. Appl. Sci.*, 11 (3), 595–611.

[2] Shinde, R., Sarkar, P.K., and Thombare, N., 2019, Soil conditioner, *Agric. Food: e-Newsl.*, 1 (10), 1–5.

[3] Rizwan, M., Rubina Gilani, S., Iqbal Durani, A., and Naseem, S., 2021, Materials diversity of hydrogel: Synthesis, polymerization process and soil conditioning properties in agricultural field, *J. Adv. Res.*, 33, 15–40.

[4] Amine, K.M., Champagne, C.P., Salmieri, S., Britten, M., St-Gelais, D., Fustier, P., and Lacroix, M., 2014, Effect of palmitoylated alginate microencapsulation on viability of *Bifidobacterium longum* during freeze-drying, *LWT - Food Sci. Technol.*, 56 (1), 111–117.

[5] Mandal, B., and Ray, S.K., 2013, Synthesis of interpenetrating network hydrogel from poly(acrylic acid-co-hydroxyethyl methacrylate) and sodium alginate: Modeling and kinetics study for removal of synthetic dyes from water, *Carbohydr. Polym.*, 98 (1), 257–269.

[6] Murphy, S.V., Skardal, A., and Atala, A., 2013, Evaluation of hydrogels for bio-printing applications, *J. Biomed. Mater. Res., Part A*, 101A (1), 272–284.

[7] Manaila, E., Craciun, G., and Calina, I.C., 2022, Sodium alginate-g-acrylamide/acrylic acid hydrogels obtained by electron beam irradiation for soil conditioning, *Int. J. Mol. Sci.*, 24 (1), 104.

[8] Naeem, A., Chengqun, Y., Hetonghui, H., Zhenzhong, Z., Weifeng, Z., and Yongmei, G., 2023, β-Cyclodextrin/chitosan-based (polyvinyl alcohol-co-acrylic acid) interpenetrating hydrogels for oral drug delivery, *Int. J. Biol. Macromol.*, 242, 125149.

[9] Wang, J., Li, H., Shen, H.X., Zhao, W., Li, Q., Wang, C.F., and Chen, S., 2023, Rapid synthesis of robust antibacterial and biodegradable hydrogels via frontal polymerization, *Gels*, 9 (12), 920.

[10] Manaila, E., Demeter, M., Calina, I.C., and Craciun, G., 2023, NaAlg-g-AA hydrogels: Candidates in sustainable agriculture applications, *Gels*, 9 (4), 316.

[11] Zhang, N., Tian, Z., Yu, Y., Wang, P., Zhou, M., and Wang, Q., 2022, Enzymatic synthesis of sodium alginate-g-poly(acrylic acid) grafting copolymers as a novel printing thickener, *Color. Technol.*, 138 (3), 278–290.

[12] Chang, A., 2015, pH-sensitive starch-g-poly(acrylic acid)/sodium alginate hydrogels for controlled release of diclofenac sodium, *Iran. Polym. J.*, 24 (2), 161–169.

[13] Athawale, V.D., and Lele, V., 2001, Recent trends in hydrogels based on starchgraft-acrylic acid: A review, *Starch - Stärke*, 53 (1), 7–13.

[14] Kowalski, G., Kijowska, K., Witczak, M., Kuterasiński, Ł., and Łukasiewicz, M., 2019, Synthesis and effect of structure on swelling properties of hydrogels based on high methylated pectin and acrylic polymers, *Polymers*, 11 (1), 114.

[15] Kalendova, P., Svoboda, L., Hroch, J., Honcova, P., Drobna, H., and Slang, S., 2021, Hydrogels based on starch from various natural sources: Synthesis and characterization, *Starch - Stärke*, 73 (9-10), 2100051.

[16] Martínez-Salcedo, S.L., Torres-Rendón, J.G., García-Enriquez, S., Anzaldo-Hernández, J., Silva-Guzmán, J.A., de Muniz, G.I.B., and Lomelí-Ramírez, M.G., 2022, Physicomechanical characterization of poly(acrylic acid-co-acrylamide) hydrogels reinforced with TEMPO-oxidized blue agave cellulose nanofibers, *Fibers Polym.*, 23 (5), 1161–1170.

[17] Kowalski, G., and Ptaszek, P., 2016, The effect of swelling time on rheological properties of hydrogels, consisting of high -amylose carboxymethyl corn starch and acrylic polymers, *Starch - Stärke*, 68 (5-6), 381–388.

[18] Toledo, P.V.O., Limeira, D.P.C., Siqueira, N.C., and Petri, D.F.S., 2019, Carboxymethyl cellulose/poly(acrylic acid) interpenetrating polymer network hydrogels as multifunctional adsorbents, *Cellulose*, 26 (1), 597–615.

[19] Zhai, X., Hu, H., Hu, M., Ji, S., Lei, T., Wang, X., Zhu, Z., Dong, W., Teng, C., and Wei, W., 2024, A nano-composite hyaluronic acid-based hydrogel efficiently antibacterial and scavenges ROS for promoting infected diabetic wound healing, *Carbohydr. Polym.*, 334, 122064.

[20] Kaur, I., and Sharma, M., 2012, Synthesis and characterization of graft copolymers of Sago starch and acrylic acid, *Starch - Stärke*, 64 (6), 441–451.

[21] Parvathy, P.C., and Jyothi, A.N., 2012, Water sorption kinetics of superabsorbent hydrogels of saponified cassava starch-graft-poly(acrylamide), *Starch - Stärke*, 64 (10), 803–812.

[22] Loureiro dos Santos, L.A., 2017, "Natural Polymeric Biomaterials: Processing and Properties" in *Reference Module in Materials Science and Materials Engineering*, Elsevier, Amsterdam, Netherlands, 1–5.

[23] Hu, C., Lu, W., Mata, A., Nishinari K., and Fang, Y., 2021, Ions-induced gelation of alginate: Mechanisms and applications, *Int. J. Biol. Macromol*., 177, 578–588.

[24] de Vasconcelos, M.C., Gomes, R.F., Sousa, A.A.L., Moreira, F.J.C., Rodrigues, F.H.A., Fajardo, A.R., and Neto, L.G.P., 2020, Superabsorbent hydrogel composite based on starch/rice husk ash as a soil conditioner in melon (*Cucumis melo* L.) seedling culture, *J. Polym. Environ*., 28 (1), 131–140.

[25] Chaudhary, J., Thakur, S., Sharma, M., Gupta, V.K., and Thakur, V.K., 2020, Development of biodegradable agar-agar/gelatin-based superabsorbent hydrogel as an efficient moisture-retaining agent, *Biomolecules*, 10 (6), 939.

[26] Singh, J., Singh, B., and Vishavnath, V., 2020, Designing starch-alginate hydrogels for controlled delivery of fungicide for the alleviation of environmental pollution, *ACS Agric. Sci. Technol*., 2 (6), 1239–1250.

[27] Suri, S., Singh, A., and Nema, P.K., 2020, Current applications of citrus fruit processing waste: A scientific outlook, *Appl. Food Res.*, 2 (1), 100050.

[28] de Andrade Rodrigues, R.M.B., da Silva Fontes, L., de Carvalho Brito, R., Barbosa, D.R.S., das Graças Lopes Citó, A.M., do Carmo, I.S., de Jesus Sousa, E.M., and Silva, G.N., 2022, A sustainable approach in the management of *Callosobruchus maculatus*: Essential oil of *Protium heptaphyllum* and its major compound D-limonene as biopesticides, *J. Plant Dis. Prot*., 129 (4), 831–841.

[29] Ibrahim, M.A., Oksanen, E.J., and Holopainen, J.K., 2004, Effects of limonene on the growth and physiology of cabbage (*Brassica oleracea* L) and carrot (*Daucus carota* L) plants, *J. Sci. Food Agric*., 84 (11), 1319–1326.

[30] Ansari, I.A., and Akhtar, M.S., 2019, "Current Insights on the Role of Terpenoids as Anticancer Agents: A Perspective on Cancer Prevention and Treatment" in *Natural Bio-active Compounds: Volume 2: Chemistry, Pharmacology and Health Care Practices*, Eds. Swamy, M.K., and Akhtar, M.S., Springer Singapore, Singapore, 53–80.

[31] Farahmandfar, R., Tirgarian, B., Dehghan, B., and Nemati, A., 2020, Comparison of different drying methods on bitter orange (*Citrus aurantium* L.) peel waste: Changes in physical (density and color) and essential oil (yield, composition, antioxidant and antibacterial) properties of powders, *J. Food Meas. Charact.*, 14 (2), 862–875.

[32] de Castro e Silva, P., de Oliveira, A.C.S., Pereira, L.A.S., Valquiria, M., Carvalho, G.R., Miranda, K.W.E., Marconcini, J.M., and Oliveira, J.E., 2020, Development of bionanocomposites of pectin and nanoemulsions of carnauba wax and neem oil pectin/carnauba wax/neem oil composites, *Polym. Compos.*, 41 (3), 858–870.

[33] Savić Gajić, I.M., Savić, I.M., and Svirčev, Z., 2023, Preparation and characterization of alginate hydrogels with high water-retaining capacity, *Polymers*, 15 (12), 2592.

[34] Azam, F., Ahmad, F., Ahmad, S., Zafar, M.S., and Ulker, Z., 2022, Preparation and characterization of alginate hydrogel fibers reinforced by cotton for biomedical applications, *Polymers*, 14 (21), 4707.

[35] Venkatachalam, K., Charoenphun, N., Nitikornwarakul, C., and Lekjing, S., 2025, Effect of sodium alginate concentration on the physicochemical, structural, functional attributes, and consumer acceptability of gel beads encapsulating tangerine peel (*Citrus reticulata* Blanco 'Cho Khun') extract, *Gels*, 11 (10), 808.

[36] Merino, D., Mansilla, A.Y., Salcedo, M.F., and Athanassiou, A., 2023, Upcycling orange peel agricultural waste for the preparation of green hydrogels as active soil conditioners, *ACS Sustainable Chem. Eng.*, 11 (29), 10917–10928.

[37] Belattmania, Z., Kaidi, S., El Atouani, S., Katif, C., Bentiss, F., Jama, C., Reani, A., Sabour, B., and

Vasconcelos, V., 2020, Isolation and FTIR-ATR and ^{1}H NMR characterization of alginates from the main alginophyte species of the Atlantic Coast of Morocco, *Molecules*, 25 (18), 4335.

[38] Dhasmana, A., Preetam, S., Malik, S., Jadon, V.S., Joshi, N., Bhandari, G., Gupta, S., Mishra, R., Rustagi, S., and Samal, S.K., 2024, Revitalizing elixir with orange peel amplification of alginate fish oil beads for enhanced anti-aging efficacy, *Sci. Rep.*, 14 (1), 20404.

[39] Ciarleglio, G., Cinti, F., Toto, E., and Santonicola, M.G., 2023, Synthesis and characterization of alginate gel beads with embedded zeolite structures as carriers of hydrophobic curcumin, *Gels*, 9 (9), 714.

[40] Szymańska-Chargot, M., Chylinska, M., Kruk, B., and Zdunek, A., 2015, Combining FT-IR spectroscopy and multivariate analysis for qualitative and quantitative analysis of the cell wall composition changes during apples development, *Carbohydr. Polym.*, 115, 93–103.

[41] Slavov, A., Ognyanov, M., and Vasileva, I., 2020, Pectic polysaccharides extracted from pot marigold (*Calendula officinalis*) industrial waste, *Food Hydrocolloids*, 101, 105545.

[42] Orsuwan, A., Shankar, S., Wang, L.F., Sothornvit, R., and Rhim, J.W., 2016, Preparation of antimicrobial agar/banana powder blend films reinforced with silver nanoparticles, *Food Hydrocolloids*, 60, 476–485.

[43] Roque-Borda, C.A., Chávez-Morán, M.R., Primo, L.M.D.G., Márquez Montesinos, J.C.E., Borges Cardoso, V.M., Saraiva, M.M.S., Marcos, C.M., Chorilli, M., Albericio, F., de la Torre, B.G., Pavan, F.R., and Meneguin, A.B., 2025, Alginate-pectin microparticles embedding self-assembling antimicrobial peptides and resveratrol for antimicrobial and anti-inflammatory applications, *Food Hydrocolloids*, 167, 111454.

[44] Ling Felicia, W.X., Rovina, K., Supri, S., Matanjun, P., Mohd Amin, S.F., and Abdul Rahman, M.N., 2025, Next-generation sodium alginate hydrogels for heavy metal ion removal: Properties, dynamic adsorption–desorption mechanisms, and sustainable application potential, *Polym. Bull.*, 82 (16), 10587–10637.

[45] Jiao, Y., Su, T., Chen, Y., Long, M., Luo, X., Xie, X., and Qin, Z., 2023, Enhanced water absorbency and water retention rate for superabsorbent polymer via porous calcium carbonate crosslinking, *Nanomaterials*, 13 (18), 2575.

[46] Van Rooyen, B., De Wit, M., Osthoff, G., Van Niekerk, J., and Hugo, A., 2023, Effect of pH on the mechanical properties of single-biopolymer mucilage (*Opuntia ficus-indica*), pectin and alginate films: development and mechanical characterisation, *Polymers*, 15 (24), 4640.

[47] Kowalski, G., Witczak, M., and Kuterasiński, Ł., 2024, Structure effects on swelling properties of hydrogels based on sodium alginate and acrylic polymers, *Molecules*, 29 (9), 1937.

[48] Hamed, R., Magamseh, K.H., Al-Shalabi, E., Hammad, A., Abu-Sini, M., Abulebdah, D.H., Tarawneh, O., and Sunoqrot, S., 2025, Green hydrogels prepared from pectin extracted from orange peels as a potential carrier for dermal delivery systems, *ACS Omega*, 10 (17), 17182–17200.

[49] Al-Mhyawi, S.R., Abdel-Tawab, N.A.H., and El Nashar, R.M., 2023, Synthesis and characterization of orange peel modified hydrogels as efficient adsorbents for methylene blue (MB), *Polymers*, 15 (2), 277.

[50] Aarstad, O., Heggset, E.B., Pedersen, I.S., Bjørnøy, S.H., Syverud, K., and Strand, B.L., 2017, Mechanical properties of composite hydrogels of alginate and cellulose nanofibrils, *Polymers*, 9 (8), 378.

[51] Nasution, H., Harahap, H., Dalimunthe, N.F., Ginting, M.H.S., Jaafar, M., Tan, O.O.H., Aruan, H.K., and Herfananda, A.L., 2022, Hydrogel and effects of crosslinking agent on cellulose-based hydrogels: A review, *Gels*, 8 (9), 568.